Applied Physics Express 4 (2011) 052102
DOI: 10.1143/APEX.4.052102

High-Power Bottom-Emitting Vertical-Cavity Surface-Emitting Lasers under Continuous-Wave, Quasi-Continuous-Wave, and Pulsed Operation

Lisen Zhang[1,2], Yongqiang Ning[1]*, Yugang Zeng[1], Li Qin[1], Yun Liu[1], Xing Zhang[1,2], Di Liu[1,2], Huawei Xu[1,2], Jinsheng Zhang[1,2], and Lijun Wang[1]

[1]*Key Laboratory of Excited State Processes, Changchun Institute of Optics, Fine Mechanics and Physics, The Chinese Academy of Sciences, Changchun, Jilin 130033, P. R. China*
[2]*Graduate School of the Chinese Academy of Science, Beijing 100039, P. R. China*

Received December 31, 2010; accepted March 29, 2011; published online April 19, 2011

The characteristics of high-power bottom-emitting vertical-cavity surface-emitting lasers (VCSELs) with an aperture of 500 μm are reported. The output power and the spectra of the device are measured at different injection currents under CW, quasi-CW, and pulsed operation. The maximum peak output power of 92 W is achieved at room temperature, which is, to the best of our knowledge, the highest value reported for a single device. The thermal effect under pulsed operation is far lower than that at the other two operation modes. © 2011 The Japan Society of Applied Physics

Vertical-cavity surface-emitting lasers (VCSELs) are becoming strong competitors to conventional edge-emitting lasers due to their advantages such as low threshold current, circular light-output mode, high packaging density for two-dimensional (2D) arrays, and single longitudinal mode emission.[1–13] A continuous-wave (CW) room-temperature output power of 1.95 W with 500 μm aperture size was reported,[14] and a record output power of 3 W with an aperture size of 350 μm was achieved in Princeton Optronics.[15] In order to further increase the output power, 2D arrays were fabricated. More than 230 W of CW power and 100 W of quasi-CW (QCW) power were obtained from a $5 \times 5\,\mathrm{mm}^2$ array chip.[16]

Due to their advantages such as high-temperature operation, intrinsic spectral stability, and high peak power, short pulse operation has wide applications in medical treatment, and industrial equipment, such as laser cutting, laser drilling, and laser welding. VCSELs have great potential in pulse operation with high peak power due to the absence of catastrophic optical damage (COD). More than 10 W pulsed power was reported from a 19-element array.[17] VCSEL arrays with 2.2 kW pulsed power were obtained.[16] 10 W of pulsed power was reported from a single device with an aperture diameter of 320 μm in 2001.[18] In another work, a peak pulsed power of 12.5 W was achieved at an injection current of 20 A from a single device with the same size above.[19] In this letter, the performances of VCSELs with a peak power of almost 100 W are reported.

A schematic view of the bottom-emitting VCSEL structure is shown in Fig. 1. The epitaxy wafer is grown on a GaAs substrate by metal-organic chemical vapor deposition (MOCVD). The wafer mainly consists of three parts: n-Distributed Bragg Reflector (DBR), active region, and p-DBR. The active region is composed of three 8-nm-thick $In_{0.2}Ga_{0.8}As$ quantum wells for an emission wavelength of about 980 nm, which are embedded in 10-nm-thick GaAs barriers. The carbon-doped p-DBR is built of 30 periods of quarter-wavelength thick $Al_{0.9}Ga_{0.1}As$/GaAs with a graded interface to reduce the series resistance. The center wavelength of p-DBR is 980 nm with a reflectivity of up to 99.9%. The Si-doped n-DBR contains only 20 pairs of quarter-wavelength thick $Al_{0.9}Ga_{0.1}As$/GaAs with a graded interface providing a reflectivity of 99.3%. This reflectivity

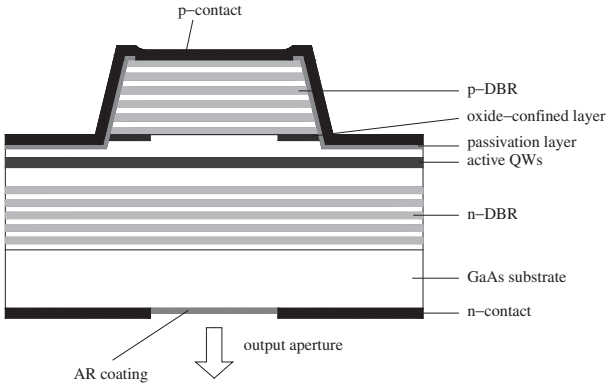

Fig. 1. Schematic diagram of the device structure.

is optimized by balancing the threshold current and the output power to realize high differential quantum efficiency under pulsed operation.

The mesa structure is formed by wet chemical etching. The samples are then exposed to high humidity in a furnace (420 °C) for the selective oxidation process. A SiO_2 layer is deposited on the mesa. After selective etching of a circular SiO_2 film, TiPtAu is evaporated on the mesa by electron beam deposition to provide a uniform current distribution. The substrate is then thinned down to 150 μm to reduce the light absorption, and an antireflection coating of HfO_2 is deposited on the GaAs substrate to form the emission window. An AuGeNi/Au film is evaporated around the HfO_2 window to form the n-contact. After rapid annealing, the wafer is cleaved into single devices and then soldered junction-down with In-solder on copper heatsinks.

The output power of VCSELs can be calculated using the following expression:

$$P_{\mathrm{out}} = \eta_{\mathrm{d}} \times \frac{h\nu}{q} \times (I - I_{\mathrm{th}}) \times \left(1 - \frac{\Delta T}{T_{\mathrm{off}}}\right), \quad (1)$$

$$\Delta T = (I^2 R_{\mathrm{s}} + I V_{\mathrm{j}}) \times R_{\mathrm{therm}} \times (1 - \eta) \times D, \quad (2)$$

where η_{d} is the differential quantum efficiency, $h\nu$ is the photon energy, q is the electronic charge, I is the injection current, I_{th} is the threshold current, ΔT is the internal temperature rise, T_{off} is the cut-off temperature, which is 170 K, R_{s} is the differential resistance, V_{j} is the junction voltage, R_{therm} is the thermal resistance, η is the power conversion efficiency, and D is a coefficient, which is

*E-mail address: yqning@126.com

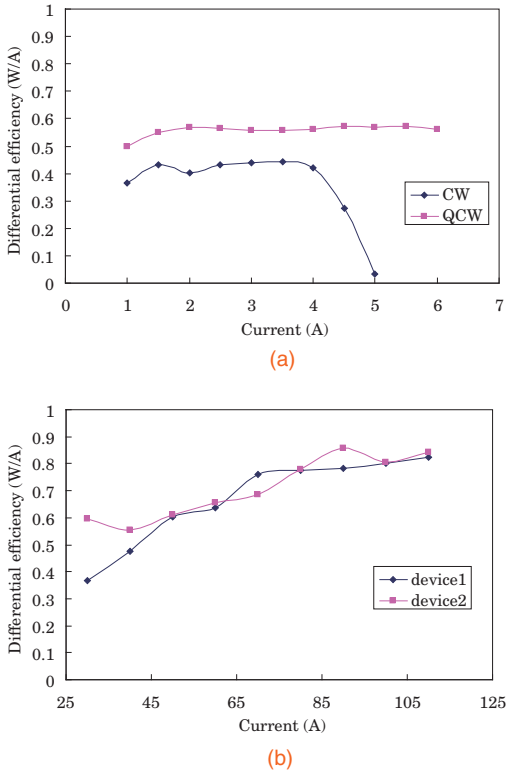

Fig. 2. Dependence of differential efficiency on injection current (a) under CW and QCW operation and (b) under pulsed operation, respectively.

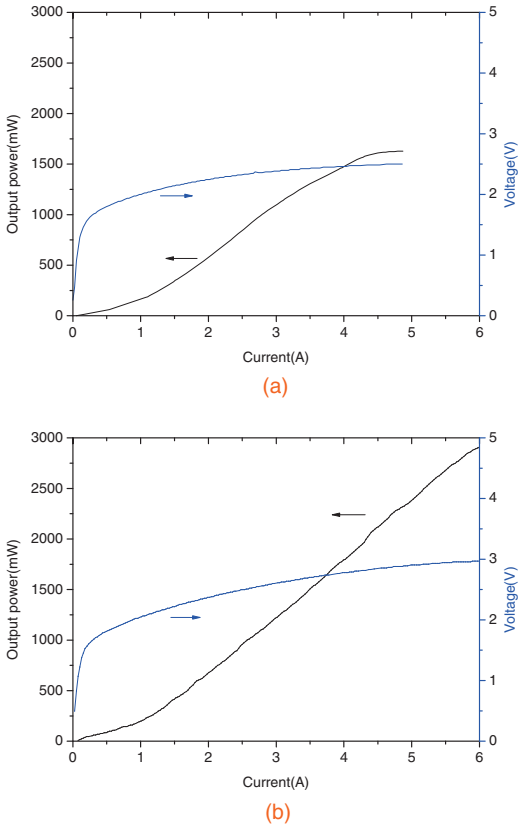

Fig. 3. L–I–V characteristics of a VCSEL single device (a) under CW operation and (b) under QCW operation.

dependent on the work condition of VCSELs. It can be seen from eqs. (1) and (2) that ΔT rises with the increase of the injection current, so the output power shows an increase and then a decrease when ΔT is high enough with the increase of current. This phenomenon was observed clearly under CW operation due to higher internal temperature rise.

The dependences of differential efficiency on injection current at CW, QCW, and pulsed operation are presented in Figs. 2(a) and 2(b) respectively. From Fig. 2(a), it is observed that the differential efficiency changes little when the injection current is less than 4 A, and it decreases rapidly at higher current because of the high internal temperature under CW operation. The differential efficiency is almost the same during the whole current range under QCW operation. Figure 2(b) shows that the differential efficiency increases with the increase of injection when the current is less than 70 A. With the current beyond 70 A, the differential efficiency remains almost constant. Under pulsed operation, the slow increase of internal temperature with the increase of injection current improves the matching between the peak gain and the center wavelength of the resonator, which results in the increase of differential quantum efficiency. Figure 2 also presents that the differential efficiency under pulsed operation is much larger than that under CW and QCW operation. From eq. (1), we can see that the differential efficiency decreases linearly with increasing ΔT. The much lower internal temperature rise ΔT causes the higher differential efficiency under pulsed operation compared with the lower differential efficiency under CW and QCW operation.

Figure 3(a) shows the CW light–current–voltage (L–I–V) characteristics of a 500-μm-diameter single device at room temperature. The threshold current and the differential resistance are 0.8 A and 0.08 Ω, respectively. A maximum output power of 1.62 W is obtained at a current of 4.5 A at room temperature. Figure 3(b) presents the QCW L–I–V characteristics of the device. The pulse width and repetition rate are 50 μs and 100 Hz, respectively. The threshold current and the differential resistance are 0.8 A and 0.12 Ω, respectively. The maximum output power of 2.89 W is achieved at a current of 6 A, which is limited by the power supply. Thermal rollover is observed under CW operation when the current is beyond 4.5 A. The reduction of the output power is not observed even at a current of 6 A under QCW operation.

The emission spectra of CW and QCW are shown in Figs. 4(a) and 4(b), which show the dependence of the peak wavelength on the injection current. The spectral full width at half maximum (FWHM) is about 1.2 nm, and remains almost the same at different currents. The thermal effect of CW operation can also be seen from the change of intensity of the lasing spectra. The redshift of the lasing wavelength from 979.18 to 984.73 nm is observed when the injection current increases from 2 to 6 A at CW operation. The redshift rate is about 1.4 nm/A, which reduces to 0.3 nm/A under QCW operation. Generally the temperature rise of the active region results in a wavelength shift of the VCSEL at a rate of about 0.06 nm/K. According to the wavelength shift shown in Fig. 4, the temperature rise of the active region under CW and QCW operation is about 90 and 20 °C, respectively. That is why thermal rollover is observed under CW operation.

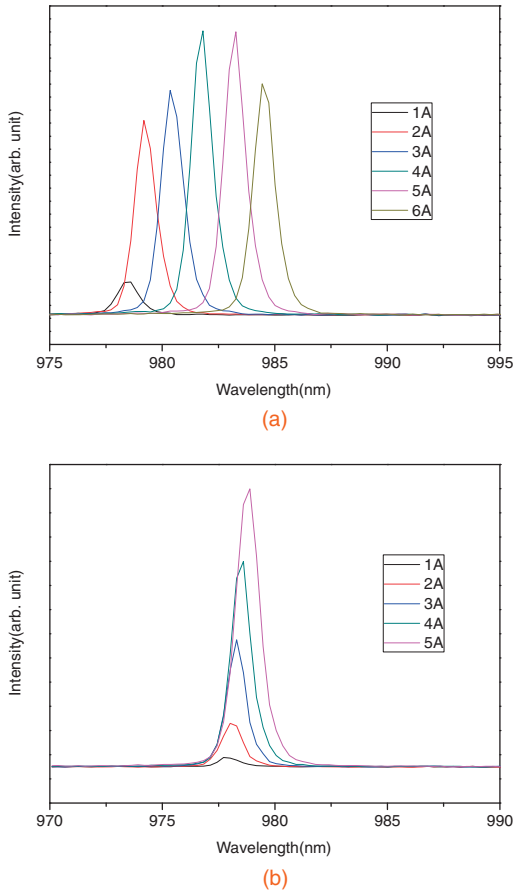

Fig. 4. Wavelength spectra at different injection currents (a) under CW operation and (b) under QCW operation.

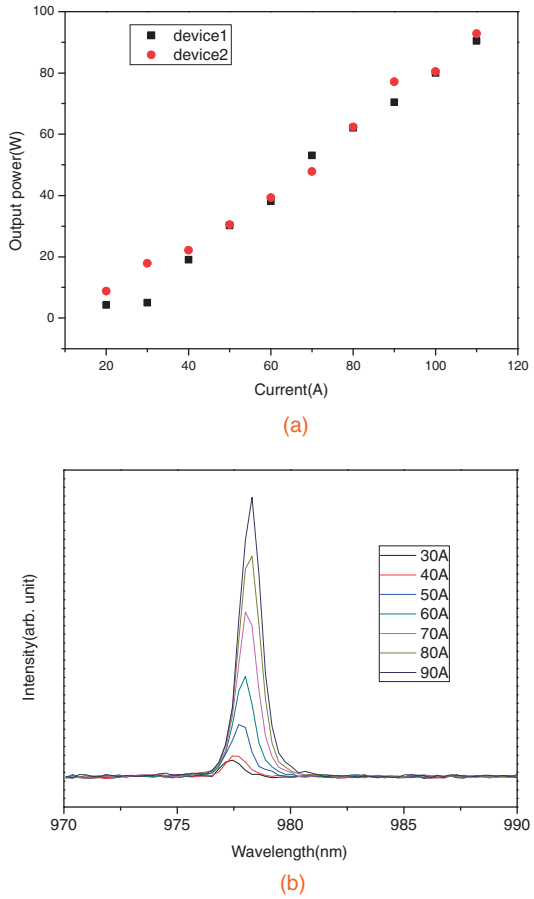

Fig. 5. (a) Dependence of output power on injection current and (b) wavelength spectra at different injection currents under pulsed operation.

In order to obtain higher power, the pulse characteristics of single devices with an aperture diameter of 500 μm are measured. The pulse width and repetition rate are 60 ns and 100 Hz, respectively. The dependence of the output power on the injection current is shown in Fig. 5(a). A maximum peak output power of 92 W is achieved at a current of 110 A, limited by the power supply, corresponding to a power density of 15 kW/cm^2. To the best of our knowledge, this is the highest value reported for a single device.

Figure 5(b) shows the dependence of the peak wavelength on the injection current. The redshift of the lasing wavelength is only 0.87 nm when the current increases from 30 to 90 A with a shift rate of 0.0145 nm/A, which is far less than the value measured under CW and QCW operation.

In conclusion, the characteristics of a single device with an aperture diameter of 500 μm are measured under CW, QCW, and short pulsed operation. From the spectra of the device, the thermal effect under pulsed operation is far lower than that under the other two operation modes. The maximum peak output power of 92 W is obtained under pulsed operation, which is the highest value reported for a single device.

Acknowledgments This work is supported by the National Natural Science Foundation of China under Grant Nos. 60636020, 60706007, 10974012, 60876036, 90923037, 11074247, and 61006054.

1) K. Iga: Jpn. J. Appl. Phys. **45** (2006) 6541.
2) K. Iga: Jpn. J. Appl. Phys. **47** (2008) 1.
3) T. Kondo, M. Arai, M. Azuchi, T. Uchida, A. Matsutani, T. Miyamoto, and F. Koyama: Jpn. J. Appl. Phys. **41** (2002) L562.
4) Y. A. Chang, F. I. Lai, H. C. Yu, H. C. Kuo, L. W. Laih, C. L. Yu, and S. C. Wang: Jpn. J. Appl. Phys. **44** (2005) L901.
5) Y. Zhang, Y. Q. Ning, L. Qin, Y. Wang, J. J. Cui, G. Y. Liu, X. Zhang, Z. F. Wang, Y. F. Sun, Y. Liu, and L. J. Wang: Appl. Opt. **49** (2010) 3793.
6) Z. F. Wang, Y. Q. Ning, Y. Zhang, J. J. Shi, X. Zhang, L. S. Zhang, W. Wang, D. Liu, Y. S. Hu, H. B. Cong, L. Qin, Y. Liu, and L. J. Wang: Opt. Express **18** (2010) 23900.
7) Y. Higuchi, K. Omae, H. Matsumura, and T. Mukai: Appl. Phys. Express **1** (2008) 121102.
8) T. C. Lu, J. T. Chu, S. W. Chen, B. S. Cheng, H. C. Kuo, and S. C. Wang: Jpn. J. Appl. Phys. **47** (2008) 6655.
9) P. B. Dayal, T. Sakaaguchi, A. Matsutani, and F. Koyama: Appl. Phys. Express **2** (2009) 092501.
10) Y. Uchiyama, T. Kondo, K.Takeda, A. Matsutani, T. Uchida, T. Miyamota, and F. Koyama: Jpn. J. Appl. Phys. **44** (2005) L214.
11) A. Onomura, M. Arai, T. Kondo, A. Matsutani, T. Miyamoto, and F. Koyama: Jpn. J. Appl. Phys. **42** (2003) L529.
12) J. H. Kim, B. S. Yoo, J. H. Shin, W. S. Han, O. K. Kwon, Y. G. Ju, and H. W. Song: Jpn. J. Appl. Phys. **43** (2004) 137.
13) R. Takigawa, E. Higurashi, T. Suga, and R. Sawada: Appl. Phys. Express **1** (2008) 112201.
14) T. Li, Y. Q. Ning, Y. F. Sun, C. Wang, J. Liu, Y. Liu, and L. J. Wang: J. Lumin. **122** (2007) 571.
15) L. A. D'Asaro, J. F. Seurin, and J. D. Wynn: Photonics Spectra **39** (2005) 64.
16) J. F. Seurin, C. L. Ghosh, V. Khalfin, A. Miglo, G. Y. Xu, J. D. Wynn, P. Pradhan, and L. A. D'Asaro: Proc. SPIE **6876** (2008) 68760D.
17) M. Miller, M. Grabherr, R. Jager, and K. J. Ebeling: IEEE Photonics Technol. Lett. **13** (2001) 173.
18) M. Miller, M. Grabherr, R. King, R. Jager, R. Michalzik, and K. J. Ebeling: IEEE J. Sel. Top. Quantum Electron. **7** (2001) 210.
19) N. Otake, K. Abe, H. Yamada, H. Wado, and Y. Takeuchi: Appl. Phys. Express **2** (2009) 052102.